Molecular Dynamical Approach to the Conformational Transition in Peptide Nanorings and Nanotubes

Masato Teranishi, Hajime Okamoto, and Kyozaburo Takeda*

Department of Electrical Engineering and Bioscience, School of Advanced Science and Engineering, Waseda University, Tokyo 169-8555, Japan

Ken-ichi Nomura, Aiichiro Nakano, Rajiv K. Kalia, and Priya Vashishta

Collaboratory for Advanced Computing and Simulations, University of Southern California, Los Angeles, California 90089

Fuyuki Shimojo

Department of Physics, Kumamoto University, Kumamoto 860-8555, Japan

Received: July 30, 2008; Revised Manuscript Received: October 30, 2008

We study the conformational transition in D,L-peptide nanorings (PNRs) and nanotubes (PNTs) computationally based on the total energy calculation. Ab initio energy calculation has been carried out to investigate the static states of PNRs, whereas the molecular dynamics (MD) calculation has been employed to examine PNRs' dynamical states. We, then, discuss the time-dependent (TD) feature via the transition process from E-type to B-type and vice versa. The conformational transition occurs easily from E-type equatorial (Eeq) to B-type axial (Bax) but is unreversible for the opposite direction because of a larger activation energy. The TD tracing of the two dihedral angles in the individual amino acid residues reveals that the conformational change propagates along the peptide skeleton ring nearly at the sound velocity. We further expand our study to the tubular forms and reveal that the PNT has an ability to produce the two kinds of homogeneous tubes, being composed of E rings (E-tube) and of B rings (B-tube), and also that these two PNRs should be mixed to produce a binary alloyed PNT.

I. Introduction

Peptide nanorings (PNRs), reported experimentally first by Ghadiri et al.,[1] are a cyclic protein synthesized artificially. These proteins have the well-defined peptide skeleton consisting of alternate sequence D- and L-amino acid residues (D,L-peptide), and provide (sub)nanometer-scale inner pores. Atoms (groups) O(=C<) and H(−N<) of the PNR's skeleton are placed in opposite directions mutually and oriented toward the outside of the molecular plane. Accordingly, the inter-ring hydrogen bonds (HBs) are induced and condense PNRs to produce a peptide nanotube (PNT) having a length of up to hundreds of micrometers.[2] Since the first synthesis of these PNRs and PNTs, Ghadiri's group has performed a number of pioneering works with their applications in mind. His group has found that the PNRs and PNTs have a potential to include not only ions and atoms but also small molecules and peptides because the internal diameter of PNRs and PNTs can be easily controlled by adjusting the number of amino acids of the component PNRs.[3,4] Thus, PNRs and PNTs are expected to be key materials in medicine as well as bio- and nanotechnology due to their excellent advantages.[5−13]

PNRs have been widely considered to have a trans-zigzag extended (E)-type backbone. However, we have recently found that PNRs also have a possibility to cause a cis-like bound (B)-type backbone. This B-type backbone is more shrunken than the E-type backbone. Hence, the B-type nanoring (B-ring) has a smaller diameter even when the number of component residues is the same as that of the E-type one (E-ring). The existence of these two types of backbone isomers is an advantage for PNRs and PNTs because the size-adjustability of the D,L-peptide nanorings is crucial in their applications in chemistry, medicine, and materials science. Therefore, we have studied the possibility of structural transition in PNRs theoretically and revealed the transition paths numerically.[14] These computational studies have been carried out by employing the ab initio approach in the static and/or stable states, but the dynamical process was then neglected in the calculations.

In this work, we study how the conformational transition occurs dynamically and discuss its time-dependent (TD) features. After describing the statical energetics between E and B rings briefly in section II, we carry out the molecular dynamics (MD) calculation and discuss the TD characteristics in the E and B conformational transition. We further expand our study to the tubular forms assembled from E-rings (E-tube) or from B-rings (B-tube) and find that both E and B tubes have the energetically stable structures (section III). The MD calculation demonstrates that the binary alloy state is possible between those E and B tubes.

II. E-Ring and B-Ring

A. Static Energetics. The stereoconformation of PNRs is well characterized by the dihedral angles ϕ ($\angle$C−N−C$^{\alpha}$−C) and ψ ($\angle$N−C$^{\alpha}$−C−N), as shown in Figure 1a. Our previous first-principles calculation demonstrates that PNR produces conformational isomers having a different geometry for the ring

* To whom correspondence should be addressed. E-mail: takeda@waseda.jp.

10.1021/jp8067975 CCC: $40.75 © 2009 American Chemical Society
Published on Web 01/09/2009

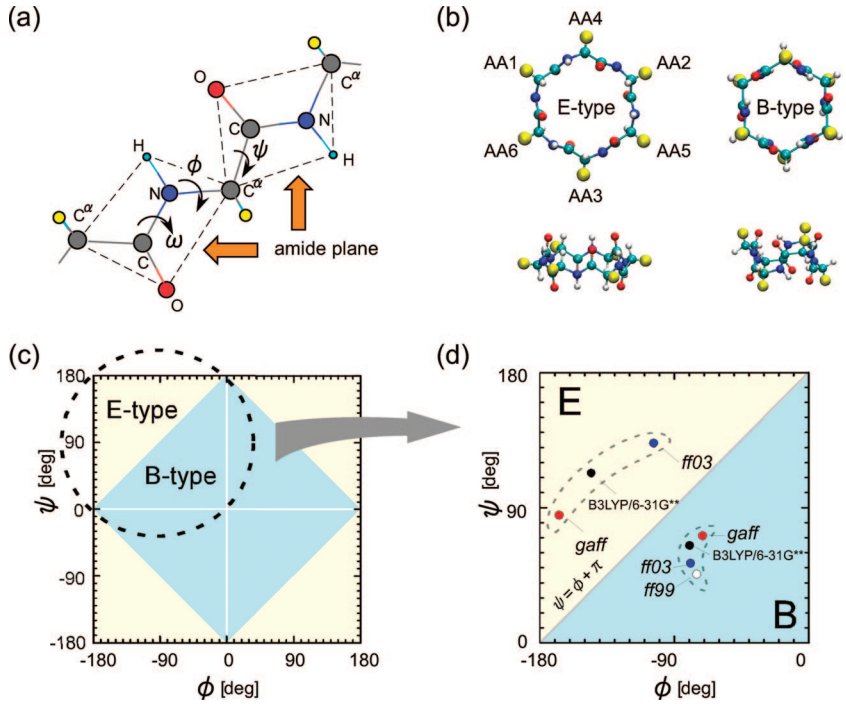

Figure 1. Geometrical parameters of the peptide sequence (a)[15] and optimized PNRs of E-type and B-type (b). The whole and the second quadrant part of the $\phi-\psi$ map are shown in (d), where we indicate the resulting ϕ and ψ of the optimized E and B rings by the black (B3LYP/6-31G**), red (AMBER/*gaff*), blue (AMBER/*ff03*), and white (AMBER/*ff99*) circles, respectively.

TABLE 1: Comparison of Dihedral Angles

	B3LYP/6-31G**		AMBER/*gaff*		AMBER/*ff03*	
	E-type	B-type	E-type	B-type	E-type	B-type
ϕ	−144.5	−78.6	−166.6	−70.7	−102.1	−78.1
ψ	114.2	65.9	85.6	70.5	133.6	52.5
ω	166.9	176.7	176.5	176.4	176.7	178.6

skeleton. One is an E-type and the other is a B-type, as shown in Figure 1b, and their dihedral angles ϕ, ψ, and ω are summarized in Table 1. The $\phi-\psi$ map of Figure 1c elucidates that a trans-zigzag extended backbone is found in the E-type PNR (E-ring) whose dihedral angles have the relation $\psi \geq \pi \pm \phi$ or $\psi \leq -(\pi \pm \phi)$. In contrast, a cis-like bound backbone is found in the B-type PNR (B-ring) because it gives the relation $-(\pi \pm \phi) < \psi < \pi \pm \phi$. This B-type backbone is more shrunken than the E-type one. Hence, B-type nanorings have a smaller diameter even when their number of component residues is the same as that of nanorings with the E-type backbone. One should note that most of the previously reported PNRs have been tacitly discussed based on the E-type conformation only, although the β-sheet-like stacking of B-type PNRs can produce a peptide nanotube (PNT) having a hollow core structure.[15]

The chirality of the amino acid residues further causes an axial or an equatorial orientation for a side chain. Consequently, the following four conformational isomers results; an E-ring having an axial side-chain orientation (Eax) and that having an equatorial one (Eeq) and a B-ring having an axial side-chain orientation (Bax) and that having an equatorial one (Beq). We illustrate these four isomers in Figure 2a. Ab initio geometry optimizations by the restricted Hartree−Fock calculation (RHF/6-31G**) and the density functional calculations (B3LYP/6-31G**) for 20 amino acid substituents indicate that there are four energetically stable local-minimum (LM) isomers in the homoresidue PNRs having a high (S_6) symmetry. Their optimized dihedral angles ϕ and ψ are those values in the area encircled by the broken line in the $\phi-\psi$ map (Figure 2b). Thus, the existence of four types of LM isomers indicates that there are six candidates for the structural transition between two nanoring isomers, Eeq ↔ Beq (**A**), Eax ↔ Bax (**B**), Beq ↔ Bax (**C**), Eeq ↔ Eax (**D**), Eeq ↔ Bax (**E**), and Eax ↔ Beq (**F**). Paths **A** and **B** cause a backbone conversion between an E-ring and a B-ring while maintaining the side-chain orientation of equatorial or axial. In contrast, paths **C** and **D** convert the side-chain orientation between equatorial and axial while maintaining the backbone conformation of the E-ring or B-ring. Of exceptional interest are the remaining **E** and **F**, where both the backbone-type and the side-chain orientation convert "simultaneously". This finding directs us to focus on the possibility of a structural transition in the peptide nanorings (isomerization) and to search for a transition path between these isomers with different diameters, leading to applications in molecular switches and atom/molecule recognition systems.

Focusing on these interesting cases, we have studied a transition path **E** (**F**) between Eeq and Bax (between Eax and Beq) by B3LYP/6-31G** with the help of the synchronous transit-guided quasi-Newton (STQN) method.[14] The calculations were performed for the simplest homo-Gly hexapeptide nanoring. In this model PNR, equatorial and axial orientations are not distinguished energetically, that is, the potential energy surface for path **E** completely coincides with that for path **F**. However, a change of the side-chain orientation can be tracked by distinguishing the substituent hydrogen atom (H^R) and the intrinsic hydrogen atom (H^α) connected to the C^α atom.

Our calculations revealed that the structural deformation between the Bax (or Beq) and the Eeq (or Eax) is not induced directly between the two LM structures having an S_6 symmetry but is achieved via new types of LM structures having a lower symmetry, such as LM1 (C_1) and LM2 (C_3) as shown in Figure 2c. LM1 is the middle structure between Eeq (S_6) and LM2 (C_3) and has an EEEBEE catenation, where E and B are defined individually at each amino acid residue by $\psi \geq \pi \pm \phi$ or $\psi \leq -(\pi \pm \phi)$ and by $-(\pi \pm \phi) < \psi < \pi \pm \phi$, respectively, as

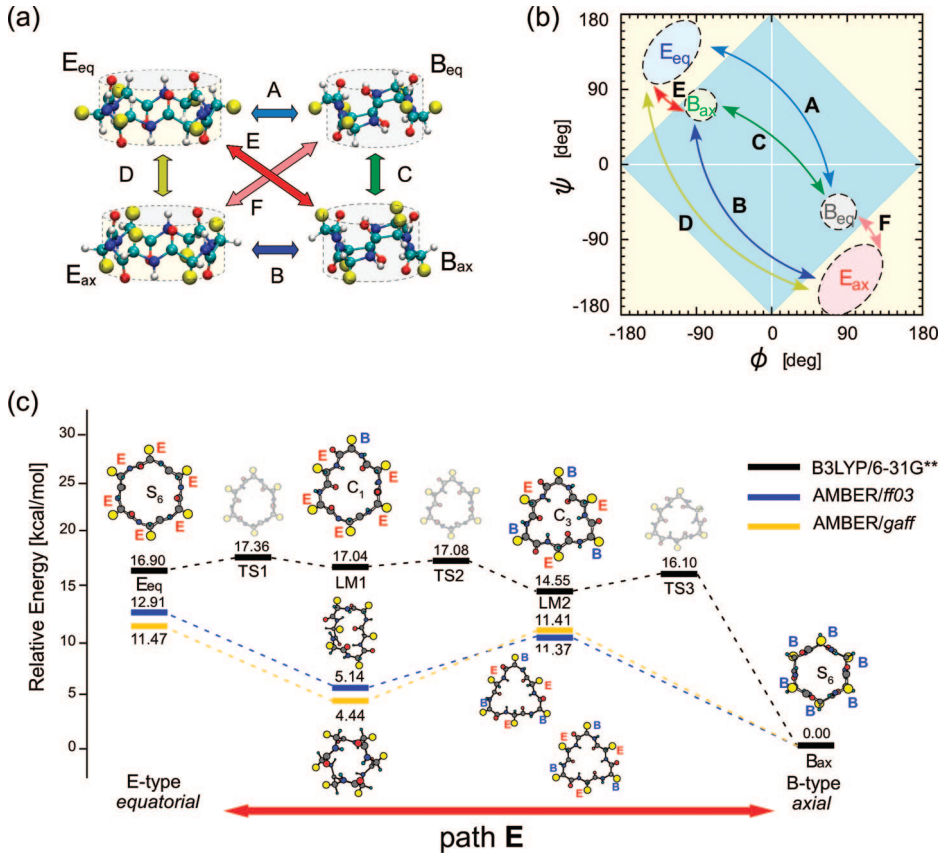

Figure 2. Illustration of four conformational isomers (a) and their transformation paths in the $\phi-\psi$ map (b). We also show the resulting transition pathway between E-type equatorial (Eeq) and B-type axial (Bax) conformations (transition E) obtained by DFT calculations (B3LYP/6-31G**) in (c). Yellow circles represent the R-group hydrogen atoms (H^R). LM and TS represent the local-minimum and transition-state structures, respectively. Panels (a), (b), and (c) are slightly modified from those by Okamoto et al.[14]

shown in Figure 1c. LM2 corresponds to the neutral structure between Bax (all B) and Eeq (all E) and has an EBEBEB alternate catenation of building blocks. One should also note the resulting trigonal ring skeleton of the LM2. The structural deformation through these LM structures is mainly produced by ϕ and ψ rotation via transition states of TS1, TS2, and TS3 (Figure 2c). Although the energy barrier from Bax to TS3 is as large as 16 kcal/mol, those among the other structures are less than 3 kcal/mol. Therefore, it is expected that the structural transition from the E-ring (Eeq) to the B-ring (Bax) is easier than that from the B-ring (Bax) to the E-ring (Eeq) in the isolated homo-Gly nanoring. Energy barriers for the structural transition will be changed by modifying the component amino acid residues, likely depending on the energy difference between the B-ring and E-ring isomers (Figure 2c). By choosing the appropriate residues that provide a small energy difference between the Eeq (Eax) and Bax (Beq), the transition barriers will be reduced.

B. Force Field Potential. We now study the dynamics in the isomerization through the conformational transition between these two isomers' E-ring and B-ring. For this subject, we carried out the empirical MD calculations by employing the AMBER program. Here, we first checked which types of the force field consistently reproduced PNR and PNT geometries and their potential energy surfaces (PESs). In Figure 1d, we give the resulting geometries of the E- and B-ring optimized by the AMBER force field calculations, where we employed the three different types of the force field *gaff* (general amber force field), *ff99*, and *ff03* (AMBER/*gaff*, AMBER/*ff99*, and AMBER/*ff03*).[16−18] Both force fields AMBER/*gaff* and AMBER/*ff03* rationally reproduce the two conformational isomers'

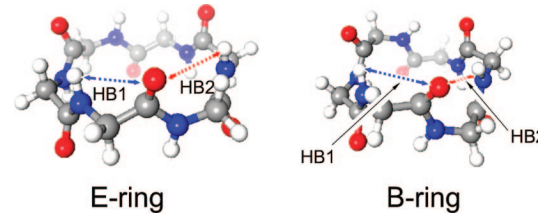

Figure 3. Illustration of the two intraring HBs of HB1 and HB2 found in the optimized E-ring and B-ring.

E-rings and B-rings having a point group symmetry of S_6, whereas the force field AMBER/*ff99* cannot reproduce an E-ring. We, therefore, exclude the use of the AMBER/*ff99* force field in the present calculation.

Figure 1d elucidates that an E-ring causes a larger ambiguity in the conformational geometry compared with that of a B-ring. As we previously revealed,[15] the PNR generates the two types of the intraring HBs as shown in Figure 3. Both of these two types of HBs are basically formed between N−H···O═C. However, one of them (HB1) is induced "within" an individual amino acid, whereas the other (HB2) is formed "over" the amino acids, as shown in Figure 3. Accordingly, the HB1 tends to produce an E-ring, whereas the HB2 favors a B-ring. In Table 2, we give the resulting interatomic distance (H···O) and angle (∠NH···O) of these HB1 and HB2 in the optimized E- and B-rings. One can find that the HB2 controlling a B-ring conformation causes a small H···O distance and a large ∠NH···O angle being near to 180°, whereas the HB1 producing an E-ring conformation causes a large interatomic distance and

TABLE 2: Comparison of the Interatomic Distance (H···O) and Angle ∠NH···O of Two Hydrogen Bonds HB1 and HB2 Found in the Optimized E- and B-Type PNRs

	E-type		B-type	
	bond length [Å]	bond angle [°]	bond length [Å]	bond angle [°]
HB1	2.32	102.6	3.81	60.8
HB2	4.23	100.5	1.93	147.6

TABLE 3: Comparison of the Conformational Geometry of the Energetically Optimized PNRs Obtained by DFT (B3LYP/6-31G) and Those by AMBER Force Field (*gaff*, *ff03*, and *ff09*) Calculations.[a]**

B3LYP/6-31G**	E-type EEEEEE	LM1 EEEBEE	LM2/EB-type EBEBEB	B-type BBBBBB
AMBER/*gaff*	E-type EEEEEE	B-type BBBBBB	EB-type EBEBEB	B-type BBBBBB
AMBER/*ff03*	E-type EEEEEE	− EBBBBB	EB-type EBEBEB	B-type BBBBBB
AMBER/*ff99*	EB-type EBEBEB	− EEEBEB	EB-type EBEBEB	B-type BBBBBB

[a] The local conformation of the individual amino acid residues is represented by symbol E or B.

a small angle. That is, HB2 is superior to HB1, and a "hard" B-ring results. This strength in HB2 reduces the geometrical ambiguity.

We further investigate which types of the AMBER force field can reproduce the reasonable PES between the E-ring and B-ring. The calculated PESs are given in Figure 2c, where we can compare them with that obtained by DFT calculation. Apart from the numerical deviation from the DFT result,[19] both of the AMBER force fileds *gaff* and *ff03* provide the reasonable PESs. We also summarize the local conformations of the individual amino acid residues in Table 3. Both of the force fields AMBER/*gaff* and AMBER/*ff03* reproduce not only the geometrical conformation of E-ring and B-ring but also the other local-minimum (LM) structures predicted by the DFT calculation. The local conformations of these LMs further correspond to those DFT results, except for the LM1.[20] Particularly, these two AMBER force field reproduce the characteristic EB triangle form (LM2) having the E and B alternating sequence well. This EBEBEB alternating conformer is an important crossing for the isomerization between the E-ring and B-ring.[14] Thus, these two AMBER potentials *gaff* and *ff03* would be quite on par in the PNR study via the present AMBER calculation. Nevertheless, we exclude the AMBER/*ff03* but employ the AMBER/*gaff* to achieve our MM and MD calculations because the former force field does not reproduce the PNT consisting of the B-type PNRs as described in section III.

C. Dynamics in Transformation. We now carry out the MD calculations in the gaseous phase under the microcanonical (NVE) ensemble owing to a simple but a direct comparison with the first-principles energetics. Our computational simulation has been continued up to 1000 ps with an interval of the time division of 1 fs. Let us first study the conformational transition from an E-ring to a B-ring because the calculated small barriers as shown in Figure 2c enforce the preferability of the conformational transition toward this EB direction rather than toward the opposite BE direction. We give the change in energies of the kinetic, potential, and total parts against time in Figure 4a−c. The present MD calculation reveals that the E-ring optimized by the AMBER/*gaff* potential cannot surmount the potential barrier(s) by an addition of kinetic energy less than 3.96kcal/mol (Figure 4a). At every moment, the PNR exchanges parts of the added kinetic energy with those of the potential energy and causes the geometrical fluctuation. Nevertheless, the time averaging of those atomistic distortions is canceled mutually around their optimized positions, and the gross deformation in the atomistic geometry hardly appears. This feature is well demonstrated by the calculated root-mean-square distance (rmsd) of the total bond length as shown in Figure 4a.

One can however find the abrupt but distinct changes in both the kinetic and potential energies when the initially applied (kinetic) energy exceeds 4.29 kcal/mol (Figure 4b). Figure 4b further demonstrates that the rmsd changes synchronically. It starts at $t_s = 613.0$ ps but finishes at $t_f = 614.8$ ps, and the stationary rmsd value results after t_f, as shown in Figure 4c. This feature indicates that some kinds of geometrical transformation occur where they propagate with a finite time of $\Delta t(= t_f - t_s) = 1.8$ ps through the PNR. We illustrate those snapshots at t_s, t_f, and t_e (stationary) on the right side. At t_s, the PNR skeleton has an all EEEEEE catenation. However, most parts of amino acids change into a B-type (BBBBEE) at t_f, and finally, the catenation of the PNR changes into a B-type. We can then estimate the averaged velocity of this propagation by $\langle v_T \rangle = \Delta L/\Delta t$. We give those values with t_s in Figure 5 by varying the initial kinetic energy. An increase in the initial kinetic energy shortens both of the starting and finish times equally. Consequently, the averaged velocity of the deformation propagation maintains its value around the sound velocity ($\sim 10^2$), irrespective of the initial kinetic energy.

How does the conformational deformation propagate through the PNR? We study this dynamical process by tracing the change in the two dihedral angles ϕ and ψ against time (Figure 6). When the initially added kinetic energy is less than 4.29 kcal/mol, the two dihedral angles ϕ and ψ for each amino acid residue fluctuate around their original positions of the optimized E-ring, but they are never forced out from the E-ring region. When the added kinetic energy exceeds 4.29 kcal/mol, those ϕ and ψ cross the boundary line of $\psi = \pi \pm \phi$ (or $\psi = -\pi \mp \phi$) and intrude into the B-ring region as shown in Figure 6a. The long-time $\phi-\psi$ map ($100 < t < 1000$ ps, Figure 6b) also indicates that these transformed ϕ and ψ never revert to the E-ring region. That is, the addition of the appropriate kinetic energy causes the unidirectional but irreversible transition from the E-ring to the B-ring (EB transition). The distinction of the two H atoms connecting to the C^{α} atom further demonstrates that this EB transition occurs via the path **E** (**F**) from Eeq to Bax (from Eax to Beq), whereas the time t_c when the dihedral angles ϕ and ψ cross the boundary line is different mutually for each amino acid residue (Figure 6b). This feature leads us to expect that the conformational deformation propagates characteristically through the PNR with a finite time, as predicted above.

Quite similarly, we have carried out our MD calculations of the conformational transition for the reverse (BE) direction. The AMBER/*gaff* potential estimates an energy difference between the stable E and B rings of 11.47 kcal/mol. The present MD calculation reveals that the activation energy is 4.29 kcal/mol for the EB transition. Accordingly, the activation energy of 15.76 kcal/mol is numerically required to cause the conformational transition from the B-ring to the E-ring (BE transition). We, then, "shake" the optimized B-ring by the kinetic energy of 16.39 kcal/mol. Figure 7a shows the change in the resulting rmsd against time. Unexpectedly, we cannot find any distinct changes as we found in the EB conformational transition. In Figure 7, we also give the change in the intraring hydrogen

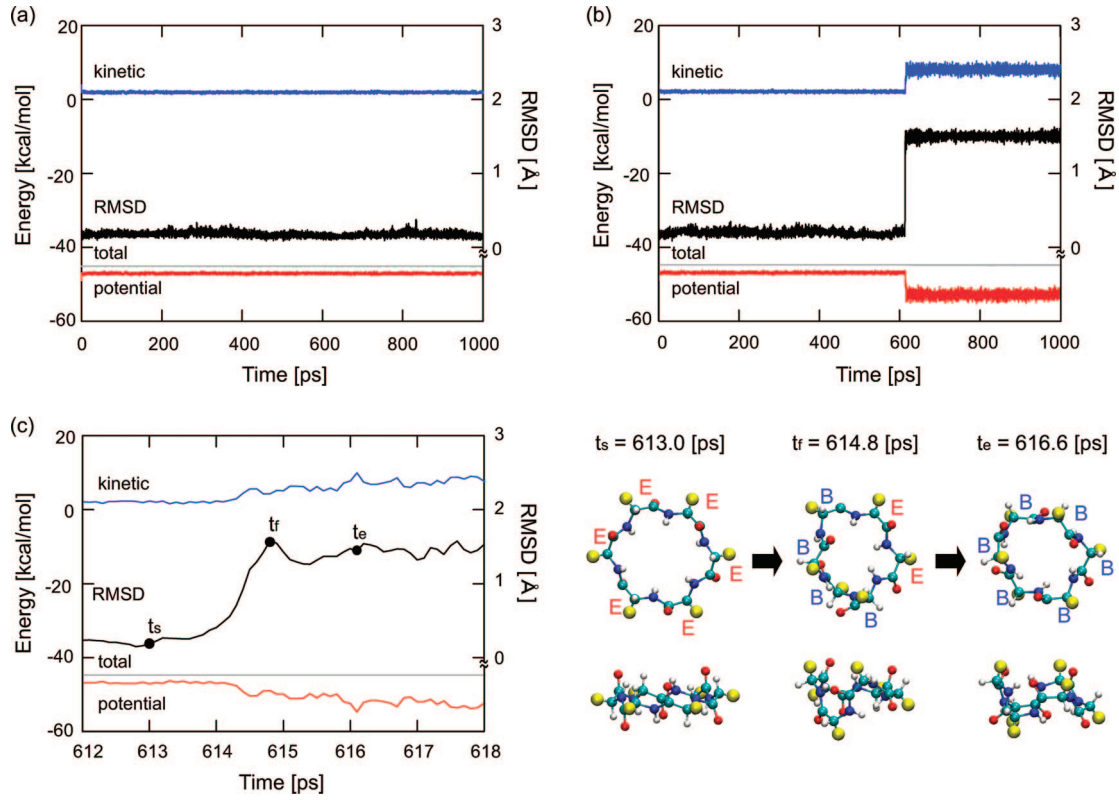

Figure 4. Change in energies of kinetic, potential, and total terms and also that in the root-mean-square distance (rmsd) of the total bond length $[(\sum(\mathbf{r}_i(t) - \mathbf{r}_i(0))^2)^{1/2}]$ against time. We vary the initial kinetic energies of 3.96 (a) and 4.29 kcal/mol (b). We magnify those changes when the conformational transition occurs in (c) with several snapshots of the molecular forms. Several snapshots are given on our Website (http://www.qms.cache.waseda.ac.jp/index-j.html).

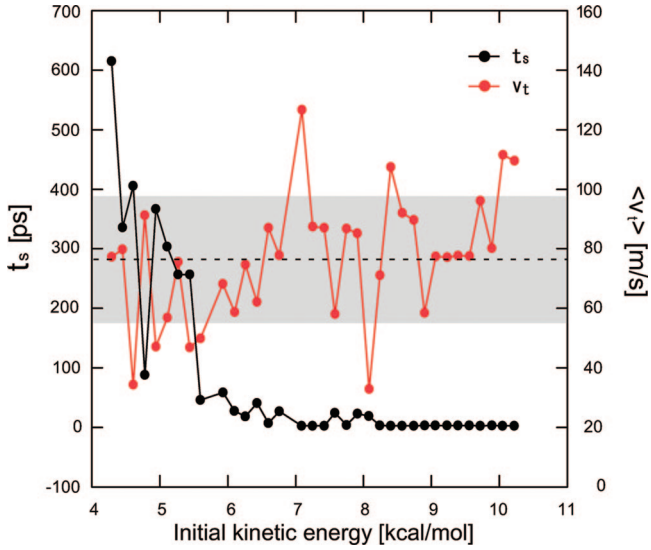

Figure 5. Change in the averaged velocity of the deformation propagation defined by $\langle v_T \rangle = \Delta L/\Delta t$ against the initially applied (kinetic) energy. The broken line indicates the averaged value of 76.52 m/s, and the gray band represents the standard deviation 20.81 m/s.

bond number (HBN) against time. Although the HBN values reduce from 6 (E-ring) to 4 at intervals, this reduction corresponds to the BE transformation occurring partly in the peptide sequence because the complete BE transformation should reduce the HBN value from 6 to 0. This partial deformation is well understood by the $\phi-\psi$ map for the individual amino acids residues as shown in Figure 7b. Several amino acid residues cross over the critical line of $-(\pi \pm \phi) < \psi < \pi \pm \phi$ at intervals, but crossings occur neither at the same time nor persistently. Thus, the "shaking" of the B-type PNR by 16.39 kcal/mol does not cause the BE conformation transition but conserves its B-ring form perpetually.

We, further, shook the optimized B-ring more strongly by the kinetic energy of 37.83 kcal/mol and calculated the values of the rmsd and HBN against time. Despite this strong "shaking", we cannot find the characteristic change in the rmsd, although the intraring HBN values are reduced to 3 frequently and to 2 or 1 occasionally. The HBN value corresponds to the number of amino acid residues having a B-type conformation in the PNR sequence. Therefore, the value HBN = 3 represents the characteristic ring where E- and B-type conformations are mixed equally. For this HBN = 3, the first-principles calculation predicts the particular triangle PNR having the EB alternating sequence (EBEBEB) as an energetically stable form (Figure 2). The detailed tracing based on the $\phi-\psi$ map, however, cannot find the corresponding EB alternating triangle ring persistently. It appears instantaneously one time up to 1000 ps. In the other times, E and B conformations are mixed equally but not alternately. Further strong shakings destroy the PNR conformation itself and change it into the meaningless form. Thus, we cannot find the BE conformational transition by the present AMBER calculation.

Why is the conformation transition irreversible between E and B rings? We should return to the $\phi-\psi$ map of Figure 2b where the six possible paths among Eeq, Beq, Eax, and Bax are indicated. Figure 2b demonstrates that the PNR having a Bax (Beq) conformation has two more adiabatical transformation paths **B** and **C** (**A** and **C**) besides the path **E** (**F**). The path **B** connects the conformational transformation from the B- to E-ring, whereas the path **C** does that between

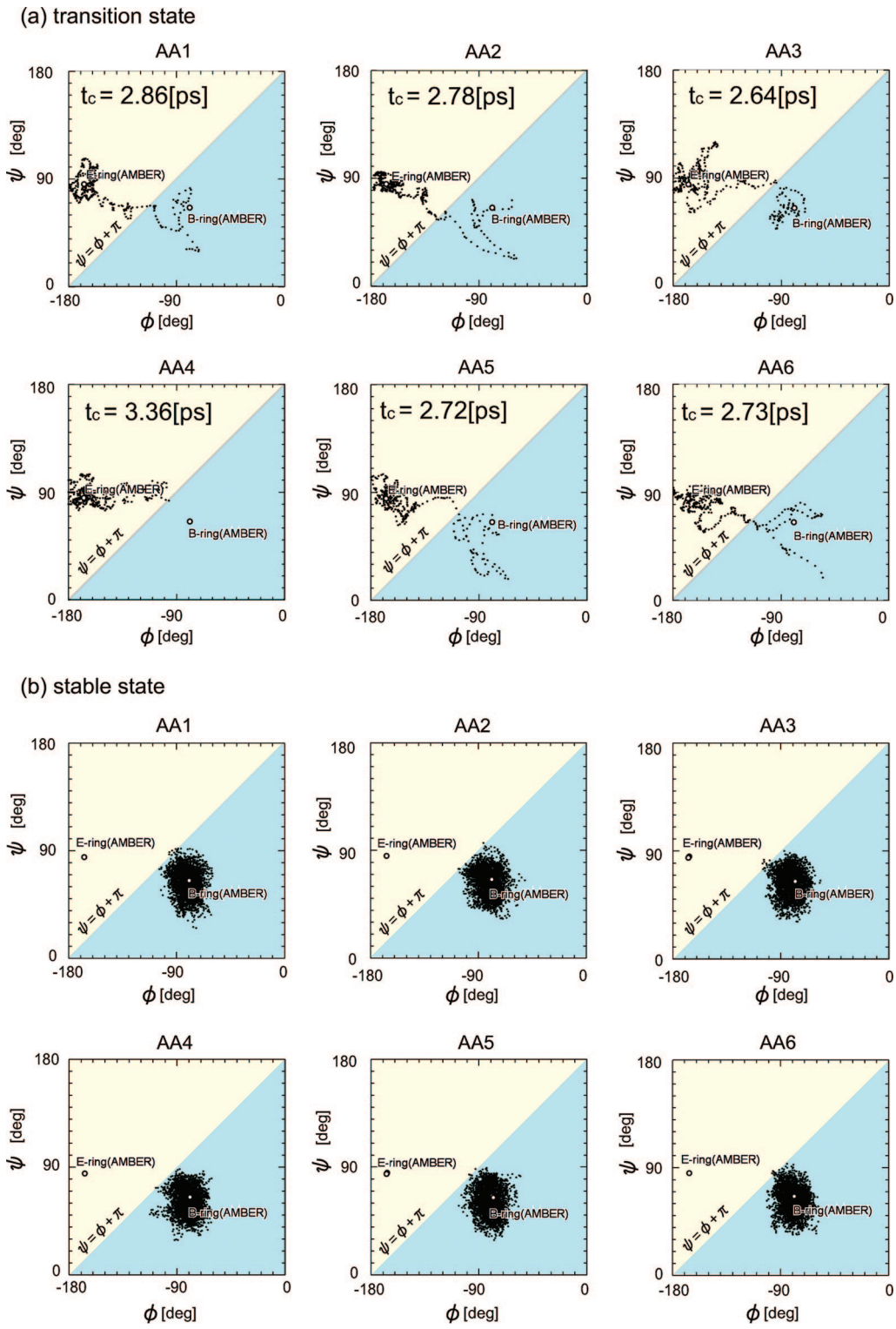

Figure 6. The $\phi-\psi$ maps of each amino acid (AA1−AA6 defined in Figure 1b) against time from $t = 0$ to 3.36 ps (a) and those from $t = 100$ to 1000 ps (b). The MD calculation has been carried out under the microcanonical ensemble, but we initially added the kinetic energy of $T = 7.09$ kcal/mol.

B-rings. We have already calculated ab initio energy profiles along these transformation pathways as shown in Figure 8,[14] where a larger energy of 22.17 kcal/mol should be required when the conformational transformation occurs along path **B** or **C**. Considering that the present MD calculation underestimates the energy values by 10 times less than the first-principles ones, a kinetic energy over 220 kcal/mol would be required for the BE conformation transition via path **B** or **C**. This is the reason why such a large kinetic energy destroys the PNR itself in the present AMBER potential.

III. E-Tube and B-Tube

A. Energetics of PNTs. We here expand our study of the molecular structure and energetics to the homogeneous PNT, where E(B)-type gly-PNRs aggregate infinitely but periodi-

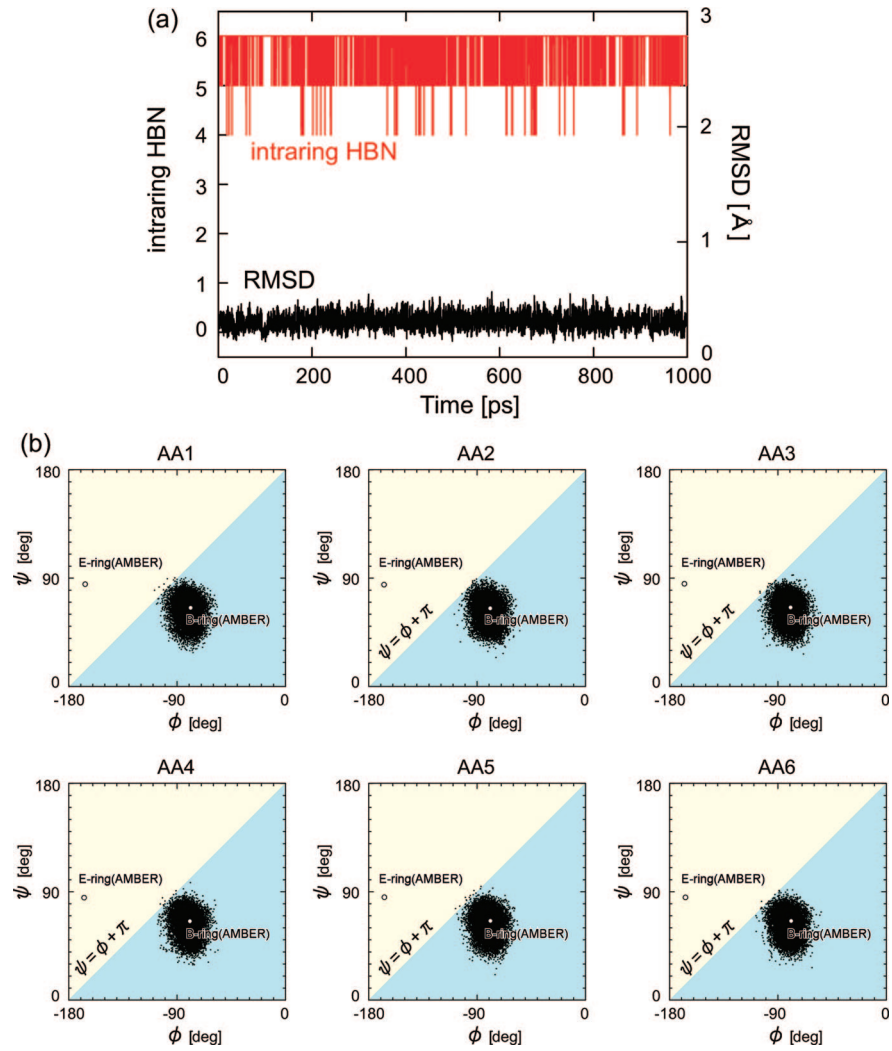

Figure 7. Change in the calculated rmsd value and hydrogen bond number (HBN) against time up to 1000 ps (a) and the time-dependent change in the two dihedral angles ϕ and ψ of each amino acid, AA1−AA6. Here, the formation of a HB is determined when the interatomic distance H···O is less than 2.5 Å and the interatomic angle ∠NH···O is within 180 ± 60°.[21] The MD calculation has been carried out under the microcanonical ensemble, but we initially added the kinetic energy of $T = 16.39$ kcal/mol.

cally in a parallel stacking manner.[22] In order to determine its optimized atomistic geometry, we here employ the periodic boundary condition of 50 PNRs and calculate the total energy while varying the inter-ring distance L (volume V of PNT). In the calculation, we set the cutoff length to 12 Å for atoms interacting through the van der Waals potential, whereas the electrostatic interactions are taken into account by the Ewald sum method. Thus, we neglect the resulting forces of less than 10^{-4} kcal/(mol·Å) in the calculation and then optimize the atomistic geometry of the whole PNT at each inter-ring distance L (V) via the AMBER/*gaff* calculation.

Figure 9a indicates the change in the resulting total energy against L, where the AMBER/*gaff* potential produces a characteristic double-minimum profile, as previous ab initio calculations have predicted.[15] Let us investigate the atomistic geometry of these optimized PNTs by tracing the changes in the two dihedral angles ϕ and ψ for the component PNRs as shown in Figure 9b. A PNT with a small inter-ring distance L has dihedral angles that are characteristic of an E-ring. With an increase in an L value, these dihedral angles approach the EB boundary line $\psi = \phi + \pi$. However, they disappear suddenly at $L =$ 5.06 Å before crossing the EB line but reappear in the B-ring area when L is larger than 5.25 Å. Thus, the PNT has an ability to produce the two kinds of homogeneous tubes, being composed of E-rings (E-tube) and of B-rings (B-tube). Figure 9a also elucidates that the energetically stable E-tube has an inter-ring distance of 4.88 Å, whereas that B-tube has 5.34 Å. These L values agree well with those first-principles results[23] of 4.90 (E-tube) and 5.31 Å (B-tube).

Figure 9b further reveals that the structural transition occurs with an abrupt discontinuity. What causes this structural transition and how? As we discussed in section II, the isolated B-ring is energetically more stable than the isolated E-ring by 11.47 kcal/mol (per ring), whereas the present PNT calculation reveals that the E-ring in the optimized E-tube is more stable than the B-ring in the optimized B-tube by 1.19 kcal/mol (per ring). This opposite trend is caused by the tube formation via the inter-ring interaction, whose crucial part is the inter-ring hydrogen bonds (HBs). As mentioned in section II, two kinds of the intraring HBs are generated in PNRs, and one of them (HB1) tends to produce an E-ring, whereas the other (HB2) favors a B-ring (Figure 3). Similarly, two kinds of HBs are induced in the inter-ring HBs. One of them is, however, formed in C^{α}−H···O═C (HB^{α}) and the other is in N−H···O═C (HB^{β}), as shown in Figure 10a. An important point is that the change in the inter-ring distance L varies the relative strength between HB^{α} and HB^{β} and further varies that between HB1 and HB2. Our calculation (Figure 9) demonstrates that a

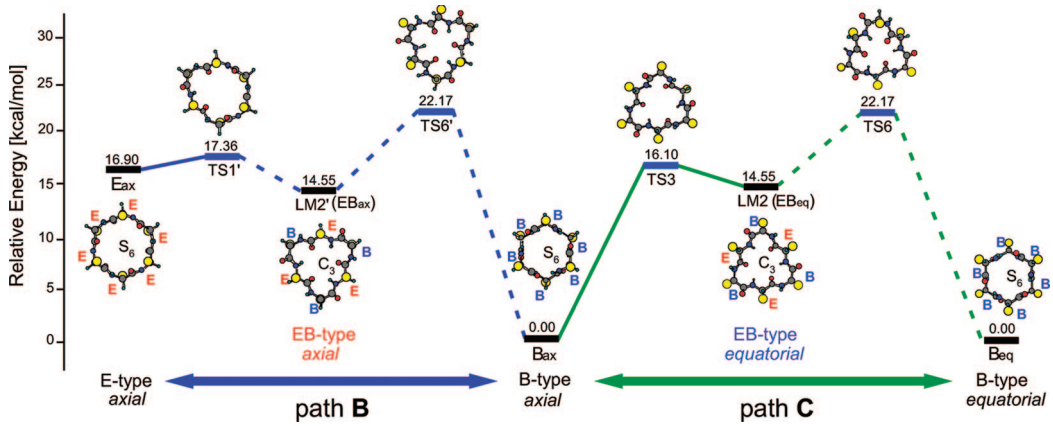

Figure 8. Calculated potential surface of the conformational transition via path **B** between Eax and Bax and that via path **C** between Beq and Bax. For the gly-PNR, path **A** between Eeq and Beq is exactly coincident with path **B**. The potential profile via path **D** has not been found yet. This figure is modified from that by Okamoto et al.[14]

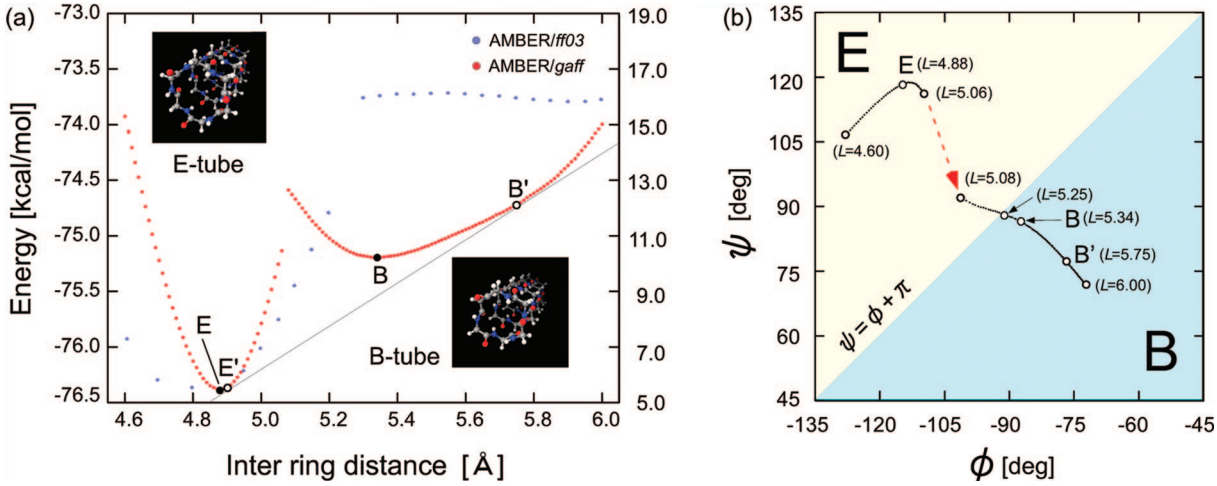

Figure 9. Change in the total energy of E- and B-type PNTs against the inter-ring distance L (volume) (a) and the trace of the dihedral angles of the component PNR indicated in the $\phi-\psi$ map (b). Symbols E and B in (a) indicate the minimum-energy point for the E- and B-tube, respectively. We also illustrate the common tangential line by the thin solid line with indication of the two tangencies E′ and B′. The indicated ϕ and ψ are those of the centered PNR in the 50 PNR unit cell of the tube because we can hardly distinguish the difference in the atomistic geometry among the constituent PNRs. The AMBER/*gaff* potential produces a characteristic double-minimum profile, whereas the AMBER/*ff03* potential does not produce the energetically stable B-tube distinctly, as shown in the figure.

homogeneous B-tube results in stacking B-rings parallelly when the inter-ring distance L is larger than 5.25 Å. The reduction in L of this B-tube moves both H(−N) and O(=C) atoms toward the direction indicated by a black arrow in Figure 10a and strengthens the inter-ring HB$^{\beta}$s. This feature is well demonstrated by the reduction in the H···O distance and the extension of the ∠N−H···O=C angle in HB$^{\beta}$, as shown in Figure 10b. One should note that this atomistic displacement simultaneously weakens the intraring HB2 but strengthens the intraring HB1. Figure 10b demonstrates that this change occurs suddenly but completely when L is less than 5.08 Å. Accordingly, the strengthened HB1s transform B-rings into E-rings, thereby producing an E-tube.

B. Binary Tube. Now, we return to the energy profile for E and B tubes in Figure 9a and discuss the possibility of the binary alloy system. Generally, the A and B binary alloy system requires the following three conditions of the thermal ($T_A = T_B$), mechanical ($p_A = p_B$), and free energy ($G_A = G_B$) equilibrium. The present energy (not free energy but the internal one) calculations have been carried out at the same temperature ($T = 0$ K), which ensures the thermal equilibrium $T_{E_{tube}} = T_{B_{tube}}$. We, then, search the situation in which the second and third equilibrium conditions are satisfied simultaneously. The resulting double-minimum profile has the common tangential line at the two tangencies E′ and B′, as shown in Figure 9a. Both of the two tubes are naturally under the same pressure when they are on this tangential line of $|p_{eq}| = |-(\partial F/\partial V)_T| = 3.73 \times 10^{-2}$ kbar, and the pressure equilibrium $p_A = p_B$ is satisfied. The resulting equilibrium pressure p_{eq} is given as

$$p_{eq} = -\frac{F_{E'} - F_{B'}}{V_{E'} - V_{B'}} \tag{1}$$

where symbols F and V are the Helmholtz's free energy and the volume of the I-th tube at each tangency E′ and B′. This equilibrium pressure further ensures that both tubes have the same Gibbs free energy ($G = F + pV$) because

$$F_{E'} + p_{eq}V_{E'} = F_{B'} + p_{eq}V_{B'} \tag{2}$$

Thus, on the tangential line, one can expect a binary system where E and B rings are mixed and form a single but E and B binary ring tube.

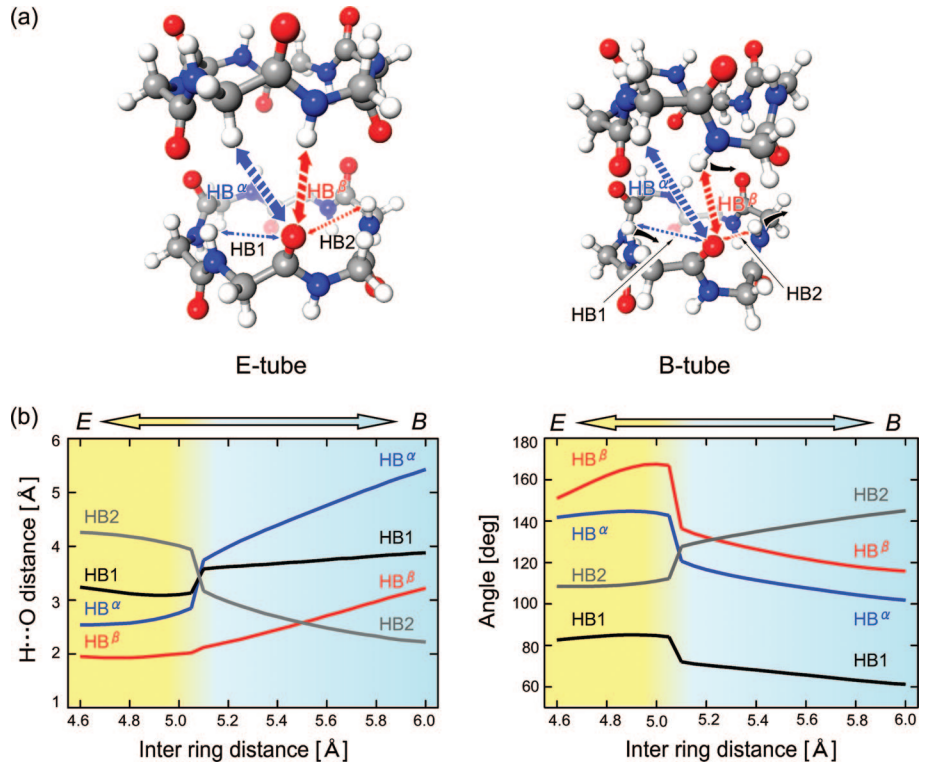

Figure 10. Illustration of the two inter-ring HBs of HB$^{\alpha}$ and HB$^{\beta}$ (a) and changes in the bond length and bond angles of those HBs (b), varying the inter-ring distance. Blue broken arrows indicate the HB of C$^{\alpha}$−H···O═C (HB1 and HB$^{\alpha}$), and red broken arrows indicate the HB of N−H···O═C (HB2 and HB$^{\beta}$).

How does the E (B)-tube lose its homogeneity by the incorporation of B (E)-rings, and how many B (E)-rings should be mixed in the binary tube when the pressure of $p_{eq} = 3.73 \times 10^{-2}$ kbar is applied uniaxially along the tube direction? We here discuss this subject by employing the molecular dynamics (MD) and the molecular mechanics (MM) approaches. First, we constructed several homogeneous E(B)-type PNTs by stacking the E′ (B′)-rings hypothetically while varying the inter-ring interval. Here, the E′ (B′)-ring is the PNR found in the optimized PNT at point E′ (B′) in Figure 9a. We then carried out the MD calculation under the NVE(∼NPE) ensemble, and investigated whether this hypothetical tube produces the stationary state or not. We also examined whether the initially set inter-ring distance is conserved in the resulting stationary state and obtained the atomistic geometry and potential of the stationary PNT at each inter-ring distance (volume). Finally, we performed the MM calculation for the MD stationary PNT and estimated the "adiabatic" potential surface to determine the energetically optimized geometry.

As shown in Figure 9a, the homogeneous E-type PNT results when $4.6 < L < 5.25$ Å, whereas that of the B-type results when $5.25 < L < 6.0$ Å. Here, we, hypothetically "synthesize" the homogeneous PNT, whose constituent PNRs are an E-type found at point E′ ($L = 4.90$ Å in Figure 9a), but the inter-ring distance L is supposed to be $L_1 = 4.985$ Å. This hypothetically elongated PNT gives the total energy of $F^*(E'/L_1) = -75.74$ kcal/mol (per ring), whose value is higher than that of the optimized E-type PNT at $L_1 = 4.985$ Å ($F^{opt/MM}(E/L_1) = -75.92$ kcal/mol per ring), as shown in Figure 11a. The unstable energy causes the atomistic forces, and all of the atoms start to move to stabilize the potential energy of the system. We, therefore, give the changes in the kinetic, potential, and total energies against the time in Figure 11a. At the initial stage, the potential and kinetic terms vacillate mutually but oppositely against the time development. This feature is because the present MD calculation has been carried out under the NVE ensemble, and then, the total energy $F^*(E'/L_1)$ is conserved during the calculation. One should, however, note that these vacillations suddenly disappear at 200 ps, and the system changes into the stationary state. The geometrical analysis based on the $\phi-\psi$ map reveals that this stationary PNT conserves the E-type ring form without causing the significant deformation or the incorporation of any other ring types except for the E-type one. The interval of the component E-rings is also conserved as initially placed as $L_1 = 4.985$ Å. Therefore, the resulting stationary potential energy $V^{stationary/MD}(E'/L_1) = -75.83$ kcal/mol is not coincident with but higher than that of the optimized homogeneous E-type PNR having the inter-ring distance of $L_1 = 4.985$ Å by 0.09 kcal/mol. That is, the system falls into the other local minimum (LM) state via another energy path. The energy difference between $V^{stationary/MD}(E'/L_1)$ and $F^{opt/MM}(E/L_1)$ is caused by the slight difference in the internal atomistic geometries between these two component E′ rings. Accordingly, we carried out the MM calculation for this stationary PNT and determined the energetically optimized PNT, where E-type PNRs still stack in parallel with the interval of $L_1 = 4.985$ Å. The obtained total energy, that is, the "adiabatic" potential, is completely coincident with that of the homogeneous E-type PNR directly optimized by the MM calculation ($F^{opt/MM}(E/L_1) = -75.92$ kcal/mol). These features are generated because the elongation in the inter-ring distance L_1 is at most 0.085 Å from the energetically optimized E′-type PNT and is small enough that the system can stabilize without incorporating B-rings.

We next set the inter-ring distance to $L_2 = 5.155$ Å and carried out the MD and MM calculations in the same way. We can observe the similar vacillations in both the potential and kinetic terms at the initial stage and also find the stationary state at ∼170 ps (Figure 11b). The resulting stationary potential is $V^{stationary/MD}(E'/L_2) = -75.62$ kcal/mol (per ring), whose value is now lower than the total energy of the optimized homoge-

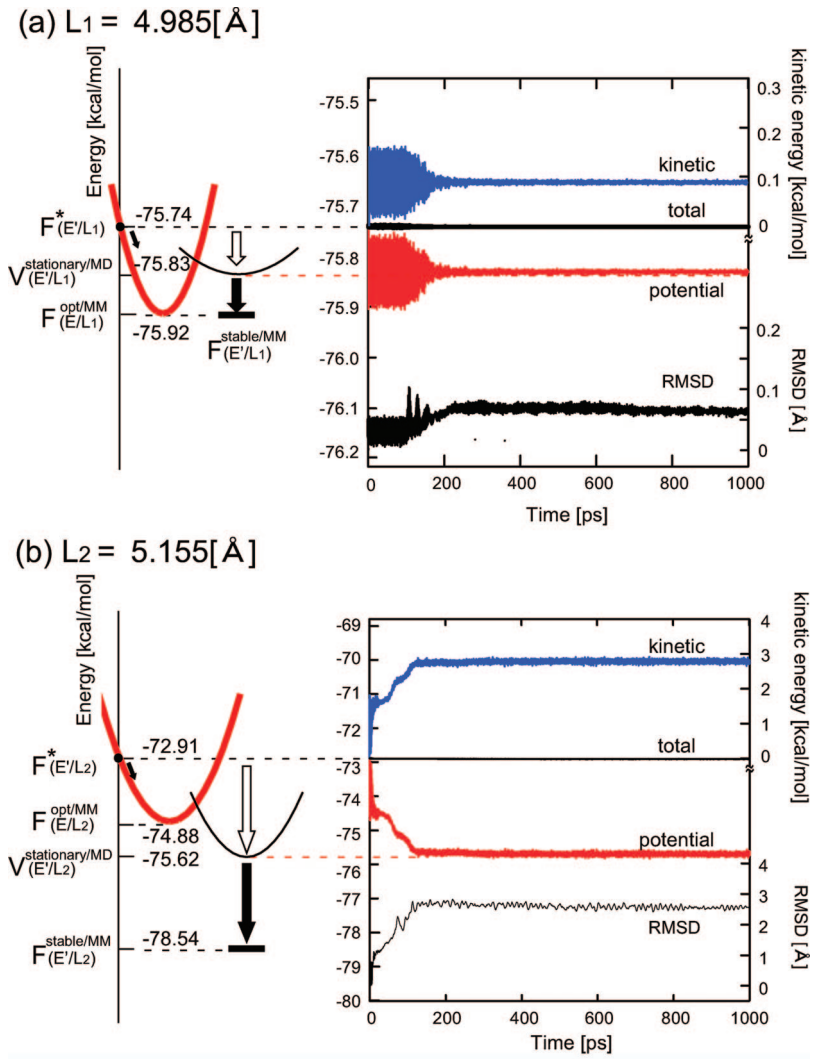

Figure 11. Changes in the potential and kinetic energy and the supposed energetics by varying the inter-ring distance $L_1 = 4.985$ Å (a) and $L_2 = 5.155$ Å (b) MM calculation with L. We also indicated the resulting change in the rmsd value. We give several calculated energy values; $F^{opt/MM}(E/L)$ means the total energy of the E-type PNT optimized by the MM calculation with L, $V^{stationary/MD}(E/L)$ is the stationary potential energy found in the MD calculation for the E-type PNT with L, and, $F^{stable/MM}(E/L)$ is the total "adiabatic potential" energy of the E-type PNT optimized by the MM calculation. Several snapshots are given on our Website (http://www.qms.cache.waseda.ac.jp/index-j.html).

neous E-type PNT having the inter-ring distance L_2 ($F^{opt/MM}(E/L_2) = -74.88$ kcal/mol). The analysis on the atomistic geometry also reveals that this stationary PNT includes B-type rings partly in addition to E-type rings, whereas the initially set inter-ring distance is conserved. Thus, the system falls into the new LM state as illustrated in Figure 11b, where E and B rings are mixed to form a binary system (EB binary tube). The MM optimization for this stationary PNT further stabilizes the total energy ($F^{stable/MM}(E'/L_2) = -78.54$ kcal/mol) and determines the "adiabatic" potential.

We extend our MD and MM calculations to study the EB binary PNT system. We initially prepared the two homogeneous tubes. One is composed of E′-rings (E′-tube), whereas the other is of B′rings (B′-tube). We then carried out MD calculations for these two tubes individually by varying the inter-ring distance L and determined the MD stationary tubes at each L. We plotted the potential energies in the stationary states of these E′ and B′ tubes individually in Figure 12a. The rational interpolation among them produces the characteristic energy profile as illustrated by the dotted line. These MD stationary tubes are not the homogeneous PNTs but include E and B rings, and the EB binary PNT results. Nevertheless, the calculated MD stationary potential energies $V^{stationary/MD}(L)$ are higher than those estimated by the common tangency line. Particularly, for the PNTs having a larger L, the stationary potential energies are even more unstable than those of the corresponding homogeneous B-type PNT.

The MM optimization, however, removes this "inconsistency". We carried out the MM optimization for these binary PNTs conjectured by the MD stationary state. The rational choice and interpolation of the resulting total energies for the MM stable PNTs produce a reasonable energy profile, which is lower than the common tangency and concludes that the most stable EB binary tube has the inter-ring distance of $L \sim 5.2$ Å. We give the resulting ratio of the composing E and B rings in the MM energetically optimized tubes against the inter-ring distance L in Figure 12b. It reveals that even the slight increase in the inter-ring distance L by 6 % from 4.9 Å changes most of the total rings into B-rings in the tube (about 90%). That is, the EB binary alloying steeply proceeds in the present E-type PNT with a slight increase in L (volume). Consequently, one can find a strong "bowing" from the Maxwell's distribution rule as shown in Figure 12b. An inherently deformable nature in the homogeneous B-tube causes this characteristic feature with the

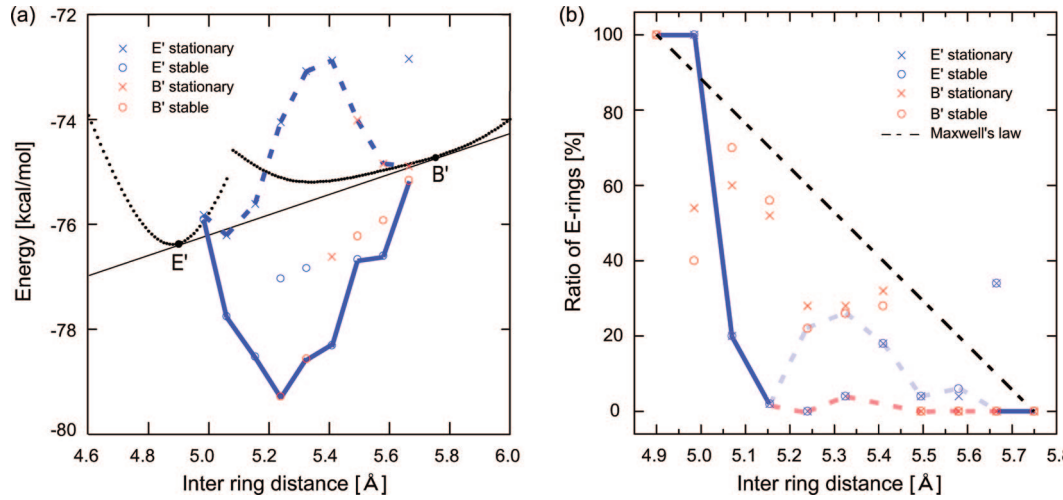

Figure 12. Energetics of the homogeneous E and B tubes and the calculated stationary and "adiabatic" potential for the EB binary alloy system (a) and the composing ratio between E and B rings (b). The rationalized MD stationary potential profile is indicated by the dotted line, whereas the reasonable MM total energy profile is indicated by the solid line in (a). We also illustrate the common tangency for two homogeneous tubes by the thin line. The simple Maxwell distribution law is indicated by the broken line in (b). We classify the ring type into E(B)-type when more than four amino acid residues locally provide an E(B)-type dihedral angle of $\psi \geq \pi \pm \phi$ or $\psi \leq -(\pi \pm \phi)$ ($-(\pi \pm \phi) < \psi < \pi \pm \phi$). We interpolate the resulting ratio found in the energetically stable PNT (solid line in (b)). However, we cannot interpolate those data reasonably when $5.2 < L < 5.5$ (broken line in (b)). When a PNR has more than the three E-type amino acid residues, we recognize that PNR belongs to a B-type.

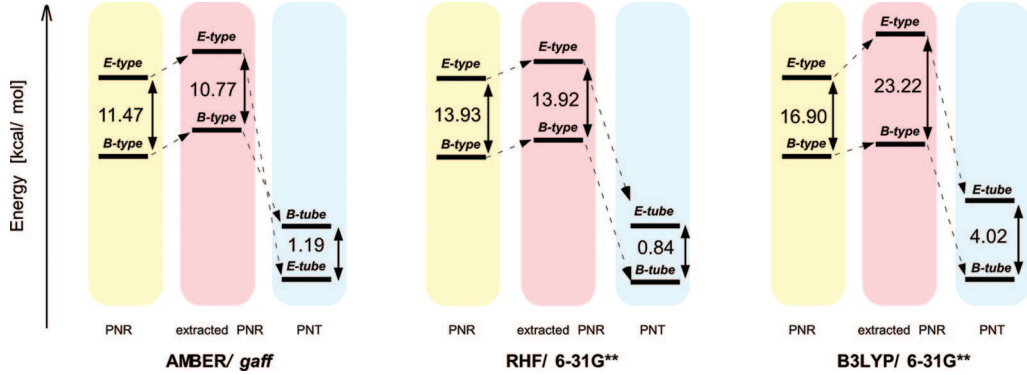

Figure 13. Comparison of the energetics of PNRs and PNTs having E-type and B-type conformations obtained by several diffferent methods, AMBER/*gaff*, RHF/6-31G**, and B3LYP/6-31G**. All of the values are given by those referred to the corresponding single PNR. At the left (yellow band), we indicate those energies for the isolated and optimized PNRs, whereas those for the optimized PNTs (per a PNR) are given at the right (blue band). We also indicate the energetics for such PNRs that are extracted from the optimized PNTs (E-tube and B-tube) at the center (red band). Because the indicated values are recalculated while maintaing their atomistic geometry, the differences between the right and center materials are caused by the inter-ring interaction.

help of the relative energetic stability between the homogeneous E and B tubes.

IV. Conclusion

• PNR produces conformational isomers having a different geometry for the ring skeleton. One is an E-type, and the other is a B-type.

• The structural deformation between the Bax (or Beq) and the Eeq (or Eax) is not induced directly between the two LM structures having an S_6 symmetry, but is achieved via new types of LM structures having a lower symmetry, such as LM1 (C_1) and LM2 (C_3).

• E-type PNR changes its conformation into the B-type one when a kinetic energy larger than 5 kcal/mol is added. The deformation of this conformational transition propagates via the peptide skeleton ring near the sound velocity ($\sim 10^2$), irrespective of the initially added kinetic energy.

• The conformational transition occurs easily from Eeq to Bax but is irreversible for the opposite direction because a larger activation energy should be required.

• The PNT has an ability to produce the two kinds homogeneous tubes, being composed of E-rings (E-tube) and B-rings (B-tube) because of the characteristic double-minimum energy profile.

• The common tangential line for the double-minimum energy profile lets us expect an existence of the binary alloy system composed of E and B rings.

• On the basis of the MD and MM calculations, we determine the "adiabatic" energy surface for the E and B binary alloy system and concluded that the EB binary alloying steeply proceeds in the present E-type PNT with an increase in L (volume).

Acknowledgment. The authors express their thanks to Prof. Masanori Takano of Waseda University for his fruitful discussion on the MD calculation, and thanks to Mr. Kazumasa Takechi for preparation of the figures. One of the authors (K.T.) also thanks to Prof. Yoshiyuki Saito of Waseda University for the discussion of the binary alloy system. Parts of the calculations have been carried out at IMS (BUNSHIKEN) Okazaki, Japan. This work was partly supported by a Grant-in-Aid for

Scientific Research on High Technology (2006) from the Ministry of Education, Culture, Sports, Science and Technology. The work at USC is partially supported by the U.S. National Science Foundation.

Appendix

Energetics. We summarize the energetics between the E-ring and B-ring or between the E-tube and B-tube in Figure 13. For PNRs, three different calculations (AMBER/*gaff*, RHF/6-31G**, and B3LYP/6-31G**) conclude that the B-ring is energetically more stable than the E-ring. On the contrary, the energetics between the E-tube and the B-tube is very delicate. The AMBER/*gaff* calculation describes the energetical stability of the E-tube, whereas both RHF/6-31G**[15] and B3LYP/6-31G** describe that of the B-tube. However, one should note the following point: The energetic stability of the B-ring is concluded by the energy difference of 12−17 kcal/mol, whereas the corresponding energy difference in PNTs is a few, or less than 1 kcal/mol. That is, one should conclude that the E-tube and B-tube would be rather "degenerate" energetically, and this degeneracy is just what PNT is expected to produce for a binary alloy of an E-tube and a B-tube.

References and Notes

(1) Ghadiri, M. R.; Granja, J. R.; Milligan, R. A.; Mcree, D. E.; Khazanovich, N. *Nature* **1993**, *366*, 324.

(2) Nakanishi, T.; Okamoto, H.; Nagai, Y.; Takeda, K.; Obataya, I.; Mihara, H.; Azehara, H.; Suzuki, Y.; Mizutani, W.; Furukawa, K.; Torimitsu, K. *Phys. Rev. B* **2002**, *66*, 165417.

(3) Granja, J. R.; Ghadiri, M. R. *J. Am. Chem. Soc.* **1994**, *116*, 10785.

(4) Sanchez-Quesada, J.; Kim, H. S.; Ghadiri, M. R. *Angew. Chem., Int. Ed.* **2001**, *40*, 2503.

(5) Fernandez-Lopez, S.; Kim, H. S.; Choi, E. C.; Delgado, M.; Granja, J. R.; Khasanov, A.; Kraehenbuehl, K.; Long, G.; Weinberger, D. A.; Wilcoxenl, K. M.; Ghadiri, M. R. *Nature* **2001**, *412*, 452.

(6) Kim, H. S.; Hartgerink, J. D.; Ghadiri, M. R. *J. Am. Chem. Soc.* **1998**, *120*, 4417.

(7) Motesharei, K.; Ghadiri, M. R. *J. Am. Chem. Soc.* **1997**, *119*, 11306.

(8) Steinem, C.; Janshoff, A.; Vollmer, M. S.; Ghadiri, M. R. *Langmuir* **1999**, *15*, 3956.

(9) Lewis, J. P.; Pawley, N. H.; Sankey, O. F. *J. Phys. Chem. B* **1997**, *101*, 10576.

(10) (a) Fukasaku, K.; Takeda, K.; Shiraishi, K *J. Phys. Soc. Jpn.* **1997**, *66*, 3387. (b) Fukasaku, K.; Takeda, K.; Shiraishi, K *J. Phys. Soc. Jpn.* **1998**, *67*, 3751.

(11) Carloni, P.; Andreoni, W.; Parrinello, M. *Phys. Rev. Lett.* **1997**, *79*, 761.

(12) Jishi, R. A.; Braier, N. C.; White, C. T.; Mintmeir, J. W. *Phys. Rev. B* **1998**, *58*, R16009.

(13) Okamoto, H.; Takeda, K.; Shiraishi, K. *Phys. Rev. B* **2001**, *64*, 115425.

(14) Okamoto, H.; Yamada, T.; Kihara, S.; Takechi, K.; Takagi, H.; Takeda, K. *J. Comput. Chem.* **2008**, DOI: 10.1002/jcc.21110.

(15) Okamoto, H.; Nakanishi, T.; Nagai, Y.; Kasahara, M.; Takeda, K. *J. Am. Chem. Soc.* **2003**, *125*, 2756.

(16) Wang, J.; Wolf, M. R.; Caldwell, W. J.; Kollman, A. P.; Case, A. D. *J. Comput. Chem.* **2004**, *25*, 1157.

(17) Duan, Y.; Wu, C.; Chowdhury, S.; Lee, C. M.; Xiong, G.; Zhang, J.; Yang, R.; Cieplak, P.; Luo, R.; Lee, T.; Caldwell, J.; Wang, J.; Kollman, P. *J. Comput. Chem.* **2003**, *24*, 1999.

(18) Wang, J.; Cieplak, P.; Kollman, A. P. *J. Comput. Chem.* **2000**, *21*, 1049.

(19) The relative energy of the Eeq conformer to the Bax conformer is calculated to be 11.47 kcal/mol by the AMBER force field, which is numerically 5.43 kcal/mol lower than that at the B3LYP/6-31G** level. The corresponding value is, however, 3.99 kcal/mol when the AMBER/*ff03* which reproduces the PNRs well, is employed. Also, that value of 2.97 kcal/mol lower is given by the HF/6-31G** calculation. Furthermore, the numerically different values (15.85 kcal/mol higher) are obtained in accordance with the different choice of the basis set (e.g., B3LYP/3-21G**) even when the DFT calculation is achieved. Thus, it can be said that Eeq is energetically more unstable than Bax, and the corresponding energy difference is almost several kcal/mol or at least less than 10 kcal/mol.

(20) The DFT calculation predicts that the LM1 has the catenation of BEEEEE, whereas the AMBER force field prefers the B conformation in the sequence as BBBBBB (AMBER/*gaff*) and EBBBBB (AMBER/*ff03*).

(21) Baker, E. N.; Hubbard, R. E. *Prog. Biophys. Mol. Biol.* **1984**, *44*, 97.

(22) We also assume that these tubes are parallelly placed with the intertube length of 60 Å in order to represent the isolated single tube having a finite volume.

(23) The sole difference is that the AMBER potential estimates the E-tube being energetically more stable than the B-tube by 1.18 kcal/mol per ring. This relation is completely opposite to that obtained by the first-principles calculation.

JP8067975